Journal of Scientific Computing

A Complete Study of the Ground State Phase Diagrams of Spin-1 Bose-Einstein Condensates in a Magnetic Field via Continuation Methods

--Manuscript Draft--

Manuscript Number:	
Full Title:	A Complete Study of the Ground State Phase Diagrams of Spin-1 Bose-Einstein Condensates in a Magnetic Field via Continuation Methods
Article Type:	Original Research
Keywords:	Spin-1 Bose-Einstein condensate; continuation method; ground state; quadratic Zeeman effect; symmetry breaking; phase transition; phase separation; phase diagram.
Corresponding Author:	I-Liang Chern TAIWAN, REPUBLIC OF CHINA
Corresponding Author Secondary Information:	
Corresponding Author's Institution:	
Corresponding Author's Secondary Institution:	
First Author:	Jen-Hao Chen, Ph.D
First Author Secondary Information:	
Order of Authors:	Jen-Hao Chen, Ph.D
	I-Liang Chern
	Weichung Wang, Ph.D
Order of Authors Secondary Information:	
Abstract:	We present a complete investigation of the ground state patterns and phase diagrams of the spin-1 Bose-Einstein condensates (BEC) confined in a harmonic or constant potential under the influence of a homogeneous magnetic field. A pseudo-arclength continuation method with parameter switching technique is developed to study the BEC systems numerically. The continuation process is performed on the parameter space consisting of the spin-independent interaction, spin-exchange interaction and the quadratic Zeeman (QZ) energy parameters. In the first stage of the parameter switching process, we fix the QZ energy term to be zero and vary the interaction parameters from zero to the desired physical values. Next, we fix the interaction parameters and vary the QZ energy parameter in both positive and negative regions. Two types of phase transitions are found, as we vary the QZ parameter. The first type is a transition from a two-component (2C) state to a three-component (3C) state. The second type is a symmetry breaking in the 3C state. Then, a phase separation of the spin components follows. In the semi-classical regime, we find that these two phase transition curves are gradually merged.

A Complete Study of the Ground State Phase Diagrams of Spin-1 Bose-Einstein Condensates in a Magnetic Field via Continuation Methods

Jen-Hao Chen[a], I-Liang Chern[b,c,d,*], Weichung Wang[b]

[a] *Department of Applied Mathematics, National Hsinchu University of Education, Hsinchu 300, Taiwan*
[b] *Institute of Applied Mathematical Sciences, National Taiwan University, Taipei 106, Taiwan*
[c] *Department of Applied Mathematics, National Chiao Tung University, Hsinchu 300, Taiwan*
[d] *Center of Mathematical Modeling and Scientific Computing, National Chiao Tung University, Hsinchu 300, Taiwan*

Abstract

We present a complete investigation of the ground state patterns and phase diagrams of the spin-1 Bose-Einstein condensates (BEC) confined in a harmonic or constant potential under the influence of a homogeneous magnetic field. A pseudo-arclength continuation method with parameter switching technique is developed to study the BEC systems numerically. The continuation process is performed on the parameter space consisting of the spin-independent interaction, spin-exchange interaction and the quadratic Zeeman (QZ) energy parameters. In the first stage of the parameter switching process, we fix the QZ energy term to be zero and vary the interaction parameters from zero to the desired physical values. Next, we fix the interaction parameters and vary the QZ energy parameter in both positive and negative regions. Two types of phase transitions are found, as we vary the QZ parameter. The first type is a transition from a two-component (2C) state to a three-component (3C) state. The second type is a symmetry breaking in the 3C state. Then, a phase separation of the spin components follows. In the semi-classical regime, we find that these two phase transition curves are gradually merged.

Keywords: Spin-1 Bose-Einstein condensate, continuation method, ground state, quadratic Zeeman effect, symmetry breaking, phase transition, phase separation, phase diagram.

*Corresponding author
Email addresses: jhchen@mail.nhcue.edu.tw (Jen-Hao Chen), chern@math.ntu.edu.tw (I-Liang Chern), wwang@ntu.edu.tw (Weichung Wang)

1. Introduction

Bose-Einstein condensates (BEC) with spin degree of freedom, called spinor BECs, have been achieved experimentally and attracted considerable interest [1, 2, 3, 4, 5] recently. By trapping all Zeeman states of an atomic species in an optical trap, these spinor BEC possess a wealth of phenomena not found in single-component condensates, including spin vortex [6], spin textures [7, 8], domain wall structure [9, 10], and spontaneous demagnetization dynamics [11, 12]. It is well known that the sign of atomic spin-exchange interaction determines the ground state property of spin-1 condensate, and leads to different quantum phases [3, 13, 14]. Moreover, under an applied external magnetic field, the spontaneous symmetry breaking in a ^{87}Rb spinor BEC has recently been observed [7]. The symmetry breaking phase transition in the ground state of the spin-1 antiferromagnetic BEC was also experimentally studied [15]. These experiments have opened up intriguing possibilities for exploring the ground state structure of spin-1 BEC under the effect between the spin-dependent interaction and the external magnetic field.

In the presence of an external magnetic field, the spin-1 BEC is subjected to the Zeeman effect [1, 16, 17, 18]. While the linear Zeeman (LZ) term has no influence on the system due to conservation of the magnetization [17], the ground state and its phase diagram of the spin-1 BEC in a magnetic field are profoundly affected by the quadratic Zeeman (QZ) term which describes the Zeeman energy difference in a spin-flip collision [1]. The competition between the QZ effect and the spin-exchange interaction results in a rich variety of ground state patterns. Numerous studies on the spin-1 BEC under positive QZ effect have been reported, including spin-domain formation [19, 20], and phase separation [17, 18]. Recently, some experiments have been performed to observe the dynamics of the spin-1 condensates of sodium atoms by using an off-resonant microwave field to rapidly switch QZ effect from positive to negative [21, 22]. This motivates us to numerically investigate the ground state patterns and phase transitions in whole range (positive and negative) of QZ effect.

The ground state structure of the spin-1 condensate in the absence of an external magnetic field has been well examined both theoretically [23, 24, 25] and numerically [26, 14, 27]. The essential feature of these works is that, in ferromagnetic systems the ground state contains all three components which are constant multiples of a scalar wave function, while the ground state contains no zero-component in antiferromagnetic systems. Moreover, no bifurcation is found on the ground state solution curve as varying the spin-independent and spin-exchange interaction parameters.

For the spin-1 BEC in the presence of a homogeneous magnetic field, Lim et al. [28] proposed a numerical method based on the normalized gradient flow to compute the ground state solution of the system. They also numerically showed that for antiferromagnetic BEC in the presence of magnetic field, there exists a critical magnetization which is the transition between two- and three-component states. In [17], the authors theoretically predicted the existence of symmetry breaking phase transition of the antiferromagnetic system without the trapping

potential. Matuszewski [18] also pointed out that in the case of harmonic trapping potentials an antiferromagnetic system can possess three distinct ground state patterns, while a ferromagnetic system possess two. However, the asymmetric solutions were drawn only schematically in their paper. In addition, the phase diagram in the negative QZ effect regime has not been studied before.

In this work, we aim to provide a complete investigation on the ground state patterns and the phase diagram of the spin-1 BECs confined in a harmonic or constant trap with positive to negative QZ effect. Based on the pseudo-arclength continuation method (PACM) [29, 30, 31], we develop a numerical scheme to study these problems. First, together with the characteristics of the ground state of the spin-1 condensate without magnetic field [14], we trace the ground state solution curve varied by the spin-independent and spin-exchange coupling constants. We next treat the QZ effect as a continuation parameter, and take the target solution under zero magnetic field as the starting state to trace the ground state solution curve subject to nonzero magnetic field. We also detect the bifurcation point in the continuation process. The results reveal a rich variety phase transition phenomena in which symmetric or asymmetric ground states are observed. These ground states also show the miscibility or immiscibility in the three hyperfine components, and possess domain wall structures. Finally, we study the phase diagrams of antiferromagnetic systems in the semi-classical regime, in which the determination of the phase transitions is a demanding task due to the nearness of the bifurcation points. In the limiting case (zero kinetic energy term), the above two phase transition curves merge. To the best of our knowledge, some results have never been reported before.

The paper is organized as follows. In the next section, we introduce the model for the spin-1 BEC subject to an external magnetic field. In Section 3, we present the numerical results of the spin-1 BEC confined in the harmonic or constant trap. The ferromagnetic or antiferromagnetic condensates with positive or negative QZ effects will be considered. In Section 4, we describe the numerical scheme based on the PACM to explore how the QZ effect and the spin-exchange interaction affect the ground state structures of the systems. Finally, conclusion of the paper is given in Section 5.

2. The Spin-1 BEC Models

At sufficiently low temperature, spin-1 atomic condensates in a nonzero homogeneous magnetic field are described by the following dimensionless Hamiltonian [16, 32, 18]:

$$\mathcal{E}[\Psi] = \int_{\mathbb{R}^3} \left[\sum_{j=-1}^{1} \psi_j^* \left(\frac{-\nabla^2}{2} + V_{ext} \right) \psi_j + \frac{1}{2} g_n |\Psi|^4 + \frac{1}{2} g_s (\Psi^* S \Psi)^2 - p \Psi^* S_z \Psi + q \Psi^* S_z^2 \Psi \right] dr. \tag{1}$$

Here, $\Psi(r) = (\psi_1(r), \psi_0(r), \psi_{-1}(r))^\top$ is the vectorial order parameter corresponding to three hyperfine sublevels of the spin, $m_F = 1, 0, -1$, at position $r = (x, y, z)$. The term V_{ext} represents the external trapping potential. The

nonlinear interaction among spin-1 condensate atoms is characterized by the spin-independent parameter g_n and spin-exchange interaction parameter g_s. For $g_n < 0$, the spin-independent interaction is attractive. For $g_n > 0$ the spin-independent interaction is repulsive. The system is ferromagnetic if $g_s < 0$ and antiferromagnetic if $g_s > 0$. The terms p and q are LZ and QZ energy parameters, respectively. These two parameters are key factors in determining the ground state patterns of the spin-1 BECs in a magnetic field. The term $S = (S_x, S_y, S_z)$ is the spin-1 Pauli operator [3, 4] and

$$S_x = \frac{1}{\sqrt{2}} \begin{pmatrix} 0 & 1 & 0 \\ 1 & 0 & 1 \\ 0 & 1 & 0 \end{pmatrix}, S_y = \frac{i}{\sqrt{2}} \begin{pmatrix} 0 & -1 & 0 \\ 1 & 0 & -1 \\ 0 & 1 & 0 \end{pmatrix}, S_z = \begin{pmatrix} 1 & 0 & 0 \\ 0 & 0 & 0 \\ 0 & 0 & -1 \end{pmatrix}. \tag{2}$$

Due to the elastic atomic collisions characterized by g_n and g_s, we have two conserved quantities. One is the normalization of the wave functions

$$N = \int_{\mathbb{R}^3} \Big(|\psi_1|^2 + |\psi_0|^2 + |\psi_{-1}|^2 \Big) dr = 1, \tag{3}$$

and the other is the total magnetization

$$M = \int_{\mathbb{R}^3} \Big(|\psi_1|^2 - |\psi_{-1}|^2 \Big) dr, \tag{4}$$

with $-1 \leq M \leq 1$. For convenience, we denote $n_j = |\psi_j|^2$ as the density of each spin component and $N_j = \int_{\mathbb{R}^3} n_j dr$ as the corresponding particle number.

By minimizing the mean field energy functional (1) subject to (3) and (4), we arrive at a set of three coupled Gross-Pitaevskii equations (CGPE)

$$\begin{cases} (\mu + \lambda)\psi_1 &= \big[\mathcal{L} + p + q + g_s(n_1 + n_0 - n_{-1})\big]\psi_1 + g_s \bar{\psi}_{-1}\psi_0^2, \\ \mu\psi_0 &= \big[\mathcal{L} + g_s(n_1 + n_{-1})\big]\psi_0 + 2g_s\psi_{-1}\bar{\psi}_0\psi_1, \\ (\mu - \lambda)\psi_{-1} &= \big[\mathcal{L} - p + q + g_s(n_0 + n_{-1} - n_1)\big]\psi_{-1} + g_s\bar{\psi}_1\psi_0^2, \end{cases} \tag{5}$$

where $\mathcal{L} = -\frac{\nabla^2}{2} + V_{ext}(r) + g_n n$ is the spin-independent part of the Hamiltonian. The Lagrange multipliers μ and λ corresponding to the constraints (3) and (4) are interpreted respectively as the chemical and magnetic potentials of the spin-1 BEC.

2.1. Settings for the numerical experiments

In this work, we consider the particular CGPE that the LZ effect is neglected and the wave functions have constant phases. For the Zeeman effect, it is well known that a spin-1 BEC in a magnetic field is subjected to the Zeeman effect. However, the LZ effect term p can be neglected due to conservation of the total magnetization in the system [7, 17, 15]. The p term can be absorbed into the magnetic potentials λ. We thus investigate the ground state structures of the spin-1 BECs under a variation of the QZ effect.

For the phases considerations, we write the wave functions $\psi_j = u_j e^{i\theta_j}$, where θ_j are constant absolute phases of the three hyperfine components. From $|\nabla\psi_j|^2 = |\nabla u_j|^2 + u_j^2|\nabla\theta_j|^2$, we see that a wave function with constant phase has least kinetic energy. In this case, the spin-exchange Hamiltonian becomes

$$\frac{1}{2}g_s(\Psi^* S\Psi)^2 = \frac{1}{2}g_s\big[(n_1-n_{-1})^2 + 2n_0(n_1+n_{-1}+2u_1u_{-1}\cos\Delta\theta)\big], \quad (6)$$

where $\Delta\theta = \theta_1 + \theta_{-1} - 2\theta_0$ is called the relative phase. To achieve minimal spin-exchange interaction, $\Delta\theta$ must be taken as 0 or π. The former is called the phase-matched (PM) state, and the latter refers to the antipahse-matched (APM) state. The PM state is energetically favorable for the ferromagnetic condensate, while the APM state is for the antiferromagnetic case [16, 19, 17, 20].

Under the above considerations, the CGPE can be rewritten as

$$\begin{cases} (\mu+\lambda)u_1 &= \mathcal{L}u_1 + qu_1 + g_s\big[n_0(u_1-\sigma u_{-1}) + u_1(n_1-n_{-1})\big] \\ \mu u_0 &= \mathcal{L}u_0 + g_s u_0(u_1-\sigma u_{-1})^2 \\ (\mu-\lambda)u_{-1} &= \mathcal{L}u_{-1} + qu_{-1} + g_s\big[n_0(u_{-1}-\sigma u_1) + u_{-1}(n_{-1}-n_1)\big], \end{cases} \quad (7)$$

where $\sigma = sign(g_s)$. We note that u_j's are real-valued functions. Since the term pM plays no role in the classification of ground states, we subtract them from the energy functional in our calculation. The corresponding reduced energy functional is

$$\begin{aligned} \tilde{\mathcal{E}}[\Psi] = \int_{\mathbb{R}^3} \Bigg[& \sum_{j=-1}^{1} u_j\Big(\frac{-\nabla^2}{2} + V_{ext}\Big)u_j \\ & + \frac{g_n}{2}\Big(n_1^2 + n_0^2 + n_{-1}^2 + 2n_1n_{-1} + 2n_0(n_1+n_{-1})\Big) \\ & + \frac{g_s}{2}\Big((n_1-n_{-1})^2 + 2n_0(u_1-\sigma u_{-1})^2\Big) + q(n_1+n_{-1})\Bigg] dr. \end{aligned} \quad (8)$$

In short, we intend to explore the ground state patterns and phase diagrams of the spin-1 BECs in nonzero magnetic field by means of the CGPE (7) with two conservations (3) and (4). We also compute the corresponding energies via reduced energy functional (8) to confirm the validity of the ground states.

In particular, we investigate both antiferromagnetic condensates ^{87}Rb ($g_n > 0$ and $g_s < 0$) and ferromagnetic condensates ^{23}Na ($g_n > 0$ and $g_s > 0$) by assuming the toal number of the cold atoms is 10^4. The spin component u_j is regarded as vanished when the *normalized* particle number N_j is less than 10^{-4}. We assume a strong transverse trapping frequency which results in an anisotropic cigar-shaped spin-1 condensate. That is, we assume $V_{ext}(x) = V_0x^2$. The ground state solutions for a quasi one-dimensional (1D) condensates are thus investigated by solving the 1D version of (7). Here, we take $V_0 = 0.5$ for the case of the harmonic trapping potential and $V_0 = 0$ for constant trapping potential. The domain Ω is chosen to be $[-L, L]$ with the grid size $h = 0.05$ in all computations. We terminate the Newton correction in the continuation process when the relative residual in the 2-norm is less than 10^{-12}.

2.2. Remarks on ground states

First, for constant trapping potential, the ground state is expected to be homogeneous away from boundaries or domain walls. They can be computed by minimizing the energy functional without the kinetic energy term. Such approximation is called the Thomas-Fermi approximation. The corresponding ground states are either a pure state or their combinations. The latter is a combination of non-overlapping pure states separated by domain walls [17, 18]. The pure states are listed below.

- A nematic state (NS) is a state in which all the atoms are in $m_F = 0$ component, that is $(0, u_0, 0)$.
- A magnetized state (MS) is a state in which all the atoms are in $m_F = +1$ or -1 component, that is $(u_1, 0, 0)$ or $(0, 0, u_{-1})$.
- A two-component (2C) state is a state in which $m_F = \pm 1$ components are populated and miscible. This usually happens in antiferromagnetic systems. For ferromagnetic systems, however, $m_F = 1, 0$ can be miscible. Such state $(u_1, u_0, 0)$ is called the $2C_{\{1,0\}}$ to distinguish from the previous $2C_{\{1,-1\}}$.
- A three-component (3C) state is a state in which all spin components are populated and miscible. Note that the 3C state is called the PM state if $\Delta\theta = 0$ and the APM state if $\Delta\theta = \pi$.

Second, we summarize some features of the ground states of the spin-1 without magnetic field as follows (see [14, 25] for more details).

- For the ferromagnetic system ($g_s < 0$), the ground state is a constant multiple of a single wave function. That is, $\Psi = (\gamma_1, \gamma_0, \gamma_{-1})\phi$, where $\gamma_i \geq 0$ and ϕ is a scalar function. Such a solution is called single mode approximation (SMA) in physics literatures. Further, the ground state preserves the population of the three components with
$$N_{3C} = (\frac{1 - N_0 + M}{2}, \frac{1 - M^2}{2}, \frac{1 - N_0 - M}{2}), \tag{9}$$
no matter how the strength of the coupling interactions change. Recently, Lin and Chern [25] also theoretically proved the validity of the single-mode approximation for the spin-1 ferromagnetic BEC, and Bao et al. [36] applied this SMA ansatz to shorten the ground state computation.
- For the antiferromagnetic system ($g_s > 0$), the ground state is a two-component (2C) state, where $\psi_0 \equiv 0$. The population of each spin component always satisfies
$$N_{2C} = (\frac{1 + M}{2}, 0, \frac{1 - M}{2}). \tag{10}$$

Finally, we have concluded that in the absence of the magnetic field, the ground state is a three-component (3C) solution ($N_j \neq 0$) if $g_s < 0$ and is a two-component (2C) solution ($N_0 = 0$) if $g_s > 0$.

3. Ground States and Phase Transitions

We present the complete study of the ground states and their phase transitions for the spin-1 BECs trapped in a harmonic or constant potential under the influence of the magnetic field. All the findings are obtained by using the continuation method proposed in Section 4. Table 1 summarizes all the scenarios considered in this study and the discoveries about the ground state patterns of the spin-1 BECs.

For a quick glance, the numerical results show that there are one or two bifurcation points along the ground state solution curve, depending on different situations (shape of the trapping potential, the sign of g_s and the sign of q). Two types of phase transitions then occur: (i) a transition from 2C state to 3C state and vise versa (in the following, named q_{cr1}), and (ii) a symmetry breaking of the ground state (named q_{cr2}). The component separation is also observed for large $|q|$ and domain walls are formed.

Detailed results are presented in the following sections. In Section 3.1, Case 1 and 2 concern the antiferromagnetic condensates (^{23}Na) with constant and harmonic trapping potential. In Section 3.2, Case 3 and 4 concern the ferromagnetic condensates (^{87}Rb) with constant and harmonic trapping potential. In Section 3.3, we assert the bifurcation diagrams in semi-classical regime numerically.

3.1. Antiferromagnetic condensates

For the antiferromagnetic system, we focus on the spin-1 ^{23}Na BECs with the spin-independent interaction $g_n = 240.8$ and the spin-exchange interaction $g_s = 7.5$ [28]. We compute the ground states with total magnetization $M = 0.3$.

Case 1:* ^{23}*Na BEC with $V_{ext}(x) = 0$. First, we study the case of the constant potential. By increasing q in the continuation algorithm, two bifurcation points ($q_{cr1} = 0.01759$ and $q_{cr2} = 0.1028$) are found with rich ground state patterns. In Fig. 1, we plot the corresponding energy curves based on the reduced energy functional (8) and label these solution branches by 1, 1-1 and 1-1-1. The densities of the starting and termination states of these solution curves are plotted in Figs. 2 to 4. We highlight some observations from these figures.

- The solution curve 1 starts from the 2C ground state of the system in zero magnetic field. From Fig. 2, we can see that this 2C state is unchanged along the entire solution curve 1. This is due to the fact that the quadratic Zeeman energy functional $\int q(n_1 + n_{-1})\,dx = qN$ is independent of the 2C state pattern. The populations N_1 and N_{-1} can be determined from N and M, see (10). This 2C state is the ground state when $q < q_{cr1}$ and becomes an excited state when $q > q_{cr1}$.

- The branch 1-1 is bifurcated from the solution curve 1 at $q = q_{cr1}$. This bifurcation leads to the population transfer from n_1 and n_{-1} to n_0, and n_{-1} is gradually depleted. From Fig. 3, we observe that the densities of each spin component are symmetric, n_0 is immiscible with n_1 and n_{-1}, and

two domain walls are formed. The ground states is this 3C (symmetric) state until q meeting the next bifurcation point q_{cr2}.

- The branch 1-1-1 is bifurcated from the branch 1-1 at $q = q_{cr2}$. On the branch 1-1-1, the corresponding solution is the ground state. It is asymmetric, and n_0 is immiscible with n_1 and n_{-1}. Eventually, in high magnetic field strength, the component n_{-1} is vanished and the ground states become immiscible MS+NS, as shown in Fig. 4. This symmetry breaking and component separation were pointed out in [17] but with only schematic structure. Here, we compute the bifurcation point q_{cr2} precisely and present details of this phase transition process.

In contrast to the case of positive q, the effect of negative QZ parameter reduces the component n_0. Thus, the simulation for $q < 0$ becomes trivial, since the ground state of the antiferromagnetic condensates in zero magnetic field is the 2C solution. The numerical results show this fact that the ground states from $q = 0$ to $q = -1$ are always the same 2C states.

We summarize the ground state patterns and their phase diagrams of the spin-1 ^{23}Na BEC in the constant potential with various strengths of the QZ effect in Table 2. The correspond energy and the particle number of u_{-1} are also listed in the table.

Case 2: ^{23}Na BEC with $V_{ext}(x) = \frac{1}{2}x^2$. We now consider the spin-1 BEC of 10^4 ^{23}Na atoms trapped in the harmonic potential. The solution curves for the case of positive q are plotted in Fig. 5. The 2C solution curve is labelled by 1 and its solution branch by 1-1. We also depict the densities of the starting and termination states of these two curves in Figs. 6 and 7. In addition, for the case of negative q, the ground states are identical 2C states, and no bifurcation is found. We demonstrate how the ground state structure changes with various q in Table 3. We also make the following remarks for this simulation.

- From Fig. 5, we observe that there is only one bifurcation ($q_{cr1} = 0.02606$). The 3C APM states bifurcate from 2C states at $q = q_{cr1}$. That is, this phase transition leads to the increase in n_0, but the depletion of n_{-1} and n_1.

- The solutions on curve 1 are identical 2C states with condition (10), as shown in Fig. 6. Note that they are the ground states when $q < q_{cr1}$. For $q > q_{cr1}$, the ground state becomes the 3C state.

- As we increase q, unlike the situation in the constant trap-potential case, there is no symmetry-breaking phase transition occurs in the harmonic trap-potential case, the ground states preserve their symmetry. This is due to a symmetric forcing of the symmetric harmonic potential. We expect that there will be a symmetry breaking when V_0 is small and/or q is large. As we further increase q, as shown in Table 3, the solutions on the branch 1-1 eventually become the symmetric MS+NS state in which n_0 is almost negligible, and n_1 and n_0 are separated. These results are in good agreement with those in [17, 18, 28].

3.2. Ferromagnetic condensates

For the case of the ferromagnetic system, we consider the spin-1 condensate of 10^4 ^{87}Rb atoms, in which $g_n = 885.4$ and $g_s = -4.1$ [28]. In contrast to the antiferromagnetic case, the ground state patterns of the ferromagnetic system are dramatically different for the negative QZ effect q. To our knowledge, there is no numerical study on the ferromagnetic spin-1 in the $q < 0$ regime.

Case 3: ^{87}***Rb BEC with*** $V_{ext}(x) = 0$. First, by employing the proposed continuation algorithm along the solution curve with parameters $q = 0$, $g_n = 885.4\tau$, $g_s = -4.1\tau$, $0 \le \tau \le 1$, we obtain the ground state of ferromagnetic condensate in zero magnetic field, which is a 3C state. Then we take q as the continuation parameter from 0 to -1. Fig. 8 is the energy curves with q ranging from 0 to -1. Figs. 9 and 10 display the starting ($q = 0$) and target ($q = -1$) states on these solution curves. The observations from these computations are highlighted as follows:

- In Fig. 8, the solutions on curve 1 are symmetric. Along this curve (with q ranging from 0 to -1), the branch 1-1 bifurcates at $q_{cr2} = -0.003452$ which has lower energy. The solutions on the branch 1-1 are asymmetric. Thus, the ground states are symmetric for $q > q_{cr2}$ and asymmetric for $q < q_{cr2}$, and q_{cr2} is a symmetry-breaking bifurcation point.
- From Figs. 9 and 10, we observe that the decrease of q suppresses n_0 for both symmetric and asymmetric solutions. As $q < q_{cr2}$, n_0 gradually depletes to zero, n_1 and n_1 are gradually immiscible and separate. Consequently, two domain walls are formed for symmetric solutions, whereas only one domain wall is form for the asymmetric ground state. This ground state is denoted by MS+MS.

For ferromagnetic condensates with positive q, we track the solution curve with q ranging from 0 to 5. The solutions start from a 3C state. As q increases, n_0 increases, but n_1 and n_{-1} decrease. Eventually, n_{-1} depletes to zero and solution is a 2C miscible state consisting components 1 and 0. We denote it by $2C_{\{1,0\}}$. Along this solution curve, the solutions are all symmetric and no bifurcation point is found. In Table 4, we collect the ground state patterns with various q for this simulation.

Case 4: ^{87}***Rb BEC with*** $V_{ext}(x) = \frac{1}{2}x^2$. In this simulation, we study the ground states of the spin-1 ^{87}Rb BEC confined in a harmonic trap. The bifurcation diagram of the ground states with negative q is depicted in Fig. 11. Similar to the case of constant potential, there is only one bifurcation ($q_{cr2} = -0.02125$) on this ground state solution curve. The q_{cr2} causes the symmetry breaking phase transition in the ground state. The properties of the ground state structure are similar to those in the constant potential. We display the starting and target states of these solution curves in Figs. 12 and 13. In Table 5, we also show the ground state patterns with various q.

3.3. Bifurcation diagram in semi-classical regime

In this subsection, we further investigate the bifurcation diagrams in semi-classical regime by considering

$$\begin{cases} (\mu+\lambda)u_1 &= \big[-\epsilon_k^2\frac{\nabla^2}{2}+g_n n+q\big]u_1+g_s\big[n_0(u_1-\sigma u_{-1})+u_1(n_1-n_{-1})\big] \\ \mu u_0 &= \big[-\epsilon_k^2\frac{\nabla^2}{2}+g_n n\big]u_0+g_s u_0(u_1-\sigma u_{-1})^2 \\ (\mu-\lambda)u_{-1} &= \big[-\epsilon_k^2\frac{\nabla^2}{2}+g_n n+q\big]u_{-1}+g_s\big[n_0(u_{-1}-\sigma u_1)+u_{-1}(n_{-1}-n_1)\big], \end{cases} \tag{11}$$

where the parameter $0<\epsilon_k\leq 1$ is the strength of the kinetic-energy term. We are interested in the variation of the bifurcation curves for various ϵ_k. In our simulations, we choose $\epsilon_k = 0.1, 0.5$ and 1. In the study below, the constant potential with $V_0 = 0$ is taken into account.

In Fig. 14, we present the ground state phase diagrams of the antiferromagnetic systems (^{23}Na) with different ϵ_k by using the proposed continuation algorithm. The two curves in these figures indicate two bifurcation points on the ground state solution curves versus magnetization M from 0.05 to 0.9. For small ϵ_k, the detection of the bifurcations becomes a demanding task due to the nearness of two phase transitions. We overcome this difficulty by tuning the step length used in Euler predictor (14). The proposed continuation algorithm thus enables us to determine precisely the bifurcations on the ground state solution curves. We highlight some observations found in these computations.

- In Fig. 14, we see that the two bifurcation curves $q_{cr1}(M)$ and $q_{cr2}(M)$ gradually merge as ϵ_k becomes smaller and smaller. We expect they merge as $\epsilon_k \to 0$.
- It is interesting to see that the bifurcation $q_{cr2}(M)$ bends backward for small M. Further, for large ϵ_k, the region between $q_{cr1}(M) < q < q_{cr2}(M)$ becomes larger and larger. This means that, for small M, it is harder and harder to break the symmetry as we increase the strength of the applied magnetic field. This is mainly due to strong homogenization effect of the kinetic energy term.

4. The Parameter Switching Continuation Methods

The discoveries presented in Section 3 are attributed by the continuation methods equipped with the parameter switching technique. Without this parameter switching technique, it would be non-trivial, if not impossible, to explore the new findings regarding the ground state phase diagrams of the spin-1 BECs in a magnetic field.

This particular continuation scheme is proposed on top of the pseudo-arclength continuation method [14, 29, 30, 31]. In the first stage, we employ the continuation algorithm proposed in [14] to trace the ground state solution curve by setting $q = 0$ and treating both g_n and g_s as continuation parameters. The target point is the ground state of the spin-1 BEC in the absence of an external magnetic field. In the second stage, the solution curve starting from the target

point in the previous stage is traced by treating q as continuation parameter, while g_n and g_s are fixed. In the study of the phase transitions, we detect the bifurcation points in the second stage.

We elaborate the continuation scheme in the following sections. For convenience, the bold face letters or symbols are used to represent matrices or vectors. The approximations of wave functions u_j and densities n_j at grid points are denoted as $\mathbf{u}_j$ and $\mathbf{n}_j$, respectively.

4.1. Pseudo-arclength continuation method (PACM)

Continuation methods are reliable and powerful tools for computing multiform solutions of a system of nonlinear equations involving one or more parameters. Various algorithms based on the continuation method have been successful in solving some challenging problems [31, 34, 14, 35, 27]. Recently, some numerical methods based on the gradient flow with discrete normalization (GFDN) have been proposed for computing ground states of spin-1 BEC systems [26, 28, 36]. The GFDN mainly computes the ground states with fixed physical parameters, while the continuation methods can be used to study not only the ground state patterns but also the bifurcation diagrams on the parameter space.

By letting $\mathbf{u} = (\mathbf{u}_1^\top, \mathbf{u}_0^\top, \mathbf{u}_{-1}^\top, \mu, \lambda)^\top \in \mathbb{R}^{3N+2}$, we write the discrete form of the CGPE (7) with the constraints (3) and (4) as the following parameterized nonlinear equation system

$$\mathbf{G}(\mathbf{u}, \tau) = \mathbf{0}, \tag{12}$$

where $\mathbf{G} : \mathbb{R}^{3N+2} \times \mathbb{R} \to \mathbb{R}^{3N+2}$. In particular, τ is the continuation parameter depending on the problem under consideration and is incorporated into (12) by setting

$$g_n = \bar{g}_n \tau,\ g_s = \bar{g}_s \tau, \text{ or } q = \bar{q}\tau,$$

where $\bar{g}_n$, $\bar{g}_s$ and $\bar{q}$ are the desired physical constants. By parametrizing the solution set $(\mathbf{u}, \tau)$ via arc-length in terms of s, we define the solution curve of (12) as

$$\mathcal{C} = \{\mathbf{x}(s) = (\mathbf{u}(s)^\top, \tau(s))^\top \mid G(\mathbf{x}(s)) = \mathbf{0},\ s \in \mathbb{R}\}. \tag{13}$$

Note that the choices of the initial points of the solution curves are crucial.

We perform the PACM by the predictor-corrector procedure based on Euler's and Newton's methods. Let $\mathbf{x}_k = \mathbf{x}(s_k) = [\mathbf{u}^\top(s_k), \tau(s_k)]^\top$ be an approximating point at the kth iteration. The Euler predictor is used to predict the next point

$$\mathbf{x}_{k+1}^{(0)} = \mathbf{x}_k + h_k \dot{\mathbf{x}}_k, \tag{14}$$

where h_k is a suitable step length and $\dot{\mathbf{x}}_k = [(\dot{\mathbf{u}}_k)^\top, \dot{\tau}_k]^\top$ is the unit tangent vector to the solution curve at the current point. To obtain $\dot{\mathbf{x}}_k$, we solve the linear system

$$\mathcal{D}\mathbf{G}(\mathbf{x}_k)\dot{\mathbf{x}}_k = \mathbf{0},$$

where

$$\mathcal{D}\mathbf{G}(\mathbf{x}_k) = [\mathbf{G}_{\mathbf{u}}(\mathbf{x}_k), \mathbf{G}_\tau(\mathbf{x}_k)] \in \mathbb{R}^{(3N+2)\times(3N+3)} \tag{15}$$

is the corresponding Jacobian matrix with respect to s.

Next, to obtain the correction vector, we use Newton method to solve the nonlinear system

$$\begin{cases} \mathbf{G}(\mathbf{u},\tau)=\mathbf{0}, \\ \dot{\mathbf{u}}_k^\top \mathbf{u}+\dot{\tau}_k\tau=\dot{\mathbf{u}}_k^\top \mathbf{u}_{k+1}^{(0)}+\dot{\tau}_k^\top \tau_{k+1}^{(0)}, \end{cases} \tag{16}$$

with the initial guess $\mathbf{x}_{k+1}^{(0)}=[\mathbf{u}_{k+1}^{(0)},\tau_{k+1}^{(0)}]$. We then solve the following augmented system

$$\begin{bmatrix} G_{\mathbf{u}}(\mathbf{x}_{k+1}^{(i)}) & G_\tau(\mathbf{x}_{k+1}^{(i)}) \\ \dot{\mathbf{u}}_i^\top & \dot{\tau}_k \end{bmatrix} \delta^{(i)} = \begin{bmatrix} G(\mathbf{x}_{k+1}^{(i)}) \\ (\mathbf{x}_{k+1}^{(i)}-\mathbf{x}_{k+1}^{(0)})\cdot\dot{\mathbf{x}}_k \end{bmatrix} \tag{17}$$

to obtain the Newton corrector

$$\mathbf{x}_{k+1}^{(i+1)}=\mathbf{x}_{k+1}^{(i)}+\delta^{(i)}. \tag{18}$$

When $\mathbf{x}_{k+1}^{(i+1)}$ satisfies the convergence criterion, we let $\mathbf{x}_{k+1}=\mathbf{x}_{k+1}^{(i+1)}$ and continue next predictor-corrector step.

4.2. The parameter-switching technique

By using the PACM described in Section 4.1, we can compute the ground state solutions of the spin-1 BEC with desired coupling constants in zero or nonzero magnetic field. On top of the PACM, we further propose the parameter-switching technique to find the ground state solutions of the spin-1 BEC in the presence of the magnetic field.

In the first stage of the parameter-switching process, we compute the ground states of the spin-1 condensate in zero magnetic field under the given strength of coupling interactions (see [14] for more details). That is, we treat g_n and g_s as the continuation parameters and track the solution curve,

$$\mathcal{C}^{(1)}=\{\mathbf{x}=(\mathbf{u}^\top,\tau)^\top \mid G(\mathbf{x})=\mathbf{0} \text{ with } g_n=\bar{g}_n\tau,\ g_s=\bar{g}_s\tau \text{ and } q=0, \text{ for } 0\le\tau\le 1\}, \tag{19}$$

which starts from the ground state solution of linear Schrödinger equation (LSE). Note that the coupling constants g_n and g_s can be adjusted by tuning the s-wave scattering length a_0 and a_2 via an appropriate setting of the Feshbach resonances [13, 37]. This provides the justification for the choice of the continuation parameters g_n and g_s.

In spin-1 condensates, the ground state patterns depend on the strength of the applied magnetic field, or equivalently, the QZ parameter q. The parameter q can be tuned experimentally via laser or microwave dressing field [15, 21, 38, 39]. Moreover, q can vary from positive to negative [21, 22]. These experimental works interest us to explore the ground state patterns for both $q>0$ and $q<0$ regime numerically.

To investigate the ground state of a spin-1 BEC numerically under the influence of an external magnetic field, we further treat the QZ parameter q as

the continuation parameter to track the solution curve

$$\mathcal{C}^{(2)} = \{\mathbf{x} = (\mathbf{u}^\top, \tau)^\top \mid G(\mathbf{x}) = \mathbf{0} \text{ with } g_n = \bar{g}_n,\ g_s = \bar{g}_s \text{ and } q = \bar{q}\tau, \text{ for } 0 \le \tau \le 1\}. \tag{20}$$

Note that $\mathcal{C}^{(2)}$ starts from the termination points at $\mathcal{C}^{(1)}$. The PACM used here is the same as that in the previous stage. However, the Jacobian matrix now depends on q and bifurcations can occur along the solution curve. We detect the bifurcation points by monitoring the smallest eigenvalues of the augmented Jacobian matrix in continuation algorithm.

5. Conclusion

Aiming at the ground state patterns and the phase diagrams of the spin-1 BECs, we have developed a numerical algorithm based on the PACM, in which the parameter-switching technique is used. By the proposed algorithm, we provide a complete investigation on the ground state patterns of spin-1 BECs over a broad range of physical parameters of interest.

For the spin-1 antiferromagnetic BEC with large enough positive QZ effect, the system undergoes two ground state phase transitions from a 2C state to a 3C symmetric state (2C→3C), then to an asymmetric phase separated state (3C→2C+NS) in the case of the constant trap. While only one phase transition (2C→3C) occurs in the case of harmonic traps and results in the symmetric phase separated ground state. Next, we investigate the spin-1 BEC in negative q regime. Particularly, for ferromagnetic condensates, the effect of negative QZ shift leads to a symmetry breaking phase transition in both constant and harmonic traps. We further study the phase transition diagrams on the (M, q) plane in the semi-classical regime. It is found that the two phase transition curves (2C→3C, 3C→2C+NS) merge as the Planck constant tends to 0. These results reveal that the proposed continuation algorithm is capable of accurately and efficiently finding all ground state patterns. Thus, a complete phase transition diagram of the spin-1 BECs in the presence of magnetic field is provided.

Acknowledgements

This work is partially supported by the National Center for Theoretical Sciences and the National Science Council of the Republic of China under contract numbers: NSC 101-2115-M-134-002 (Chen), NSC 102-2115-M-009-013 (Chern), and NSC 100-2628-M-002-011-MY4 (Wang).

References

[1] J. Stenger, S. Inouye, D. Stamper-Kurn, H.-J. Miesner, A. Chikkatur, W. Ketterle, Spin domains in ground-state Bose–Einstein condensates, Nature 396 (6709) (1998) 345–348.

[2] D. Stamper-Kurn, M. Andrews, A. Chikkatur, S. Inouye, H.-J. Miesner, J. Stenger, W. Ketterle, Optical confinement of a Bose-Einstein condensate, Physical Review Letters 80 (10) (1998) 2027.

[3] T.-L. Ho, Spinor Bose condensates in optical traps, Physical review letters 81 (4) (1998) 742.

[4] T. Isoshima, K. Machida, T. Ohmi, Spin-domain formation in spinor Bose-Einstein condensation, Physical Review A 60 (6) (1999) 4857.

[5] I. Bloch, J. Dalibard, W. Zwerger, Many-body physics with ultracold gases, Reviews of Modern Physics 80 (3) (2008) 885.

[6] A. Leanhardt, Y. Shin, D. Kielpinski, D. Pritchard, W. Ketterle, Coreless vortex formation in a spinor Bose-Einstein condensate, Physical review letters 90 (14) (2003) 140403.

[7] L. Sadler, J. Higbie, S. Leslie, M. Vengalattore, D. Stamper-Kurn, Spontaneous symmetry breaking in a quenched ferromagnetic spinor bose–einstein condensate, Nature 443 (7109) (2006) 312–315.

[8] Y. Kawaguchi, H. Saito, M. Ueda, Can spinor dipolar effects be observed in Bose-Einstein condensates?, Physical review letters 98 (11) (2007) 110406.

[9] H. Nistazakis, D. Frantzeskakis, P. Kevrekidis, B. Malomed, R. Carretero-González, A. Bishop, Polarized states and domain walls in spinor Bose-Einstein condensates, Physical Review A 76 (6) (2007) 063603.

[10] Z.-D. Li, Q.-Y. Li, P.-B. He, J.-Q. Liang, W. Liu, G. Fu, Domain-wall solutions of spinor Bose-Einstein condensates in an optical lattice, Physical Review A 81 (1) (2010) 015602.

[11] S. Hoshi, H. Saito, Symmetry-breaking magnetization dynamics of spinor dipolar Bose-Einstein condensates, Physical Review A 81 (1) (2010) 013627.

[12] B. Pasquiou, E. Maréchal, G. Bismut, P. Pedri, L. Vernac, O. Gorceix, B. Laburthe-Tolra, Spontaneous demagnetization of a dipolar spinor bose gas in an ultralow magnetic field, Physical Review Letters 106 (25) (2011) 255303.

[13] M.-S. Chang, Q. Qin, W. Zhang, L. You, M. S. Chapman, Coherent spinor dynamics in a spin-1 Bose condensate, Nature Physics 1 (2) (2005) 111–116.

[14] J.-H. Chen, I.-L. Chern, W. Wang, Exploring ground states and excited states of spin-1 Bose-Einstein condensates by continuation methods, Journal of Computational Physics 230 (6) (2011) 2222–2236.

[15] D. Jacob, L. Shao, V. Corre, T. Zibold, L. De Sarlo, E. Mimoun, J. Dalibard, F. Gerbier, Phase diagram of spin-1 antiferromagnetic Bose-Einstein condensates, Physical Review A 86 (6) (2012) 061601.

[16] W. Zhang, S. Yi, L. You, Mean field ground state of a spin-1 condensate in a magnetic field, New Journal of Physics 5 (1) (2003) 77.

[17] M. Matuszewski, T. J. Alexander, Y. S. Kivshar, Excited spin states and phase separation in spinor Bose-Einstein condensates, Physical Review A 80 (2) (2009) 023602.

[18] M. Matuszewski, Ground states of trapped spin-1 condensates in magnetic field, Physical Review A 82 (5) (2010) 053630.

[19] M. Matuszewski, T. J. Alexander, Y. S. Kivshar, Spin-domain formation in antiferromagnetic condensates, Physical Review A 78 (2) (2008) 023632.

[20] J. Mur-Petit, Spin dynamics and structure formation in a spin-1 condensate in a magnetic field, Physical Review A 79 (6) (2009) 063603.

[21] E. M. Bookjans, A. Vinit, C. Raman, Quantum phase transition in an antiferromagnetic spinor Bose-Einstein condensate, Physical Review Letters 107 (19) (2011) 195306.

[22] A. Vinit, E. Bookjans, C. S. de Melo, C. Raman, Antiferromagnetic spatial ordering in a quenched one-dimensional spinor gas, Physical review letters 110 (16) (2013) 165301.

[23] W. Bao, Y. Zhang, Dynamical laws of the coupled gross-pitaevskii equations for spin-1 Bose-Einstein condensates, Methods and Applications of Analysis 17 (1) (2010) 49–80.

[24] D. Cao, I.-L. Chern, J.-C. Wei, On ground state of spinor Bose-Einstein condensates, NoDEA: Nonlinear Differential Equations and Applications 18 (4) (2011) 427–445.

[25] L. Lin, I.-L. Chern, Proofs of some simplified characterizations of the ground states of spin-1 Bose-Einstein condensates, arXiv preprint arXiv:1102.0832.

[26] W. Bao, F. Y. Lim, Computing ground states of spin-1 Bose-Einstein condensates by the normalized gradient flow, SIAM Journal on Scientific Computing 30 (4) (2008) 1925–1948.

[27] Y.-S. Wang, C.-S. Chien, A two-parameter continuation method for computing numerical solutions of spin-1 Bose–Einstein condensates, Journal of Computational Physics 256 (2014) 198–213.

[28] F. Y. Lim, W. Bao, Numerical methods for computing the ground state of spin-1 bose-einstein condensates in a uniform magnetic field, Physical Review E 78 (6) (2008) 066704.

[29] H. D. Mittelmann, A pseudo-arclength continuation method for nonlinear eigenvalue problems, SIAM journal on numerical analysis 23 (5) (1986) 1007–1016.

[30] E. L. Allgower, K. Georg, Numerical continuation methods, Vol. 13, Springer-Verlag Berlin, 1990.

[31] Y.-C. Kuo, W.-W. Lin, S.-F. Shieh, W. Wang, A minimal energy tracking method for non-radially symmetric solutions of coupled nonlinear schrödinger equations, Journal of Computational Physics 228 (21) (2009) 7941–7956.

[32] D. R. Romano, E. J. V. de Passos, Population and phase dynamics of f= 1 spinor condensates in an external magnetic field, Physical Review A 70 (4) (2004) 043614.

[33] M. Bayindir, B. Tanatar, Z. Gedik, Bose-Einstein condensation in a one-dimensional interacting system due to power-law trapping potentials, Physical Review A 59 (2) (1999) 1468.

[34] C.-S. Chien, S.-L. Chang, B. Wu, Two-stage continuation algorithms for bloch waves of Bose-Einstein condensates in optical lattices, Computer Physics Communications 181 (10) (2010) 1727–1737.

[35] Y.-C. Kuo, S.-F. Shieh, W. Wang, Rotational quotient procedure: A tracking control continuation method for pdes on radially symmetric domains, Computer Physics Communications 183 (4) (2012) 998–1001.

[36] W. Bao, I.-L. Chern, Y. Zhang, Efficient numerical methods for computing ground states of spin-1 bose-einstein condensates based on their characterizations, Journal of Computational Physics 253 (2013) 189–208.

[37] E. Van Kempen, S. Kokkelmans, D. Heinzen, B. Verhaar, Interisotope determination of ultracold rubidium interactions from three high-precision experiments, Physical review letters 88 (9) (2002) 093201.

[38] F. Gerbier, A. Widera, S. Fölling, O. Mandel, I. Bloch, Resonant control of spin dynamics in ultracold quantum gases by microwave dressing, Physical Review A 73 (4) (2006) 041602.

[39] S. Leslie, J. Guzman, M. Vengalattore, J. D. Sau, M. L. Cohen, D. Stamper-Kurn, Amplification of fluctuations in a spinor Bose-Einstein condensate, Physical Review A 79 (4) (2009) 043631.

[40] B. Seaman, L. Carr, M. Holland, Effect of a potential step or impurity on the Bose-Einstein condensate mean field, Physical Review A 71 (3) (2005) 033609.

[41] K. Kasamatsu, M. Tsubota, Multiple domain formation induced by modulation instability in two-component Bose-Einstein condensates, Physical review letters 93 (10) (2004) 100402.

[42] M. Moreno-Cardoner, J. Mur-Petit, M. Guilleumas, A. Polls, A. Sanpera, M. Lewenstein, Predicting spinor condensate dynamics from simple principles, Physical review letters 99 (2) (2007) 020404.

[43] M. Yasunaga, M. Tsubota, Ferromagnetic resonance in spinor dipolar Bose-Einstein condensates, Physical Review A 83 (1) (2011) 013618.

Table 1: Summaries of the ground state patterns of the spin-1 BECs.

BEC	Potential	QZ effect	Ground state patterns
^{23}Na	Constant (Case 1)	$q > 0^*$	2C $\rightarrow$ 3C $\rightarrow$ 2C+NS $\rightarrow$ MS+NS
		$q = 0$	2C
		$q < 0^\dagger$	2C
	Harmonic (Case 2)	$q > 0^\ddagger$	2C $\rightarrow$ 3C $\rightarrow$ 2C+NS $\rightarrow$ MS+NS
		$q = 0$	2C
		$q < 0^\dagger$	2C
^{87}Rb	Constant (Case 3)	$q > 0^*$	3C $\rightarrow$ 2C$_{\{1,0\}}$
		$q = 0$	3C
		$q < 0^\dagger$	3C $\rightarrow$ 2C+NS $\rightarrow$ MS+MS+NS $\rightarrow$ MS+MS
	Harmonic (Case 4)	$q > 0^\ddagger$	3C $\rightarrow$ 2C$_{\{1,0\}}$
		$q = 0$	3C
		$q < 0^\dagger$	3C $\rightarrow$ 2C+NS $\rightarrow$ MS+MS+NS $\rightarrow$ MS+MS

* Only schematic drawings in literatures [17] and never been numerically studied.
† Only been observed in experiments [21, 22] and never been numerically studied.
‡ Agree with literatures [17, 18, 28].

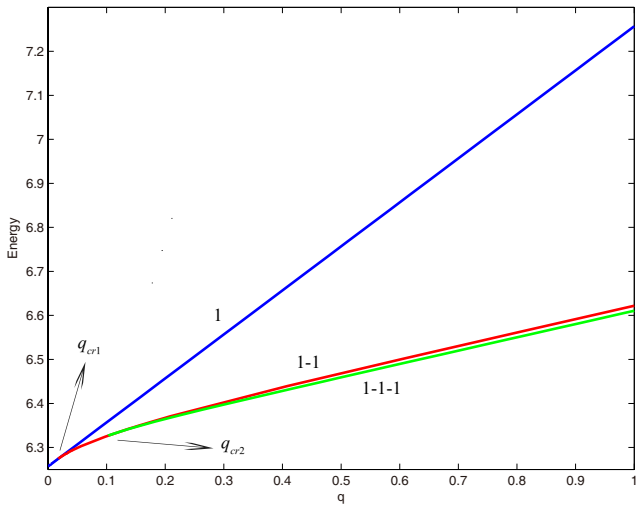

Figure 1: (Case 1) Energy curves of ^{23}Na with $M = 0.3$ in the constant potential. There are two bifurcation points $q_{cr1} = 0.01759$ and $q_{cr2} = 0.1028$.

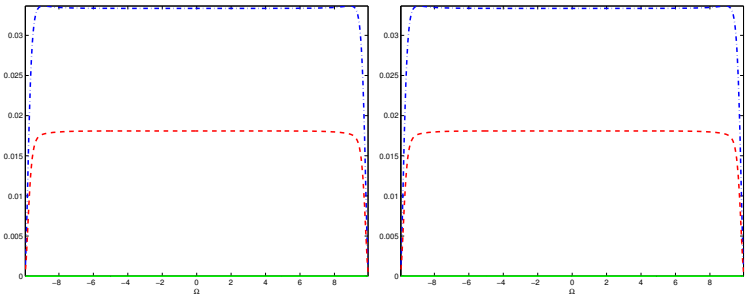

Figure 2: (Case 1) Densities of the starting state $q = 0$ (left) and the target state $q = 1$ (right) of curve 1 in Fig. 1. The $m_F = 1, 0, -1$ components are depicted by blue dash-dotted, green solid and red dashed lines, respectively.

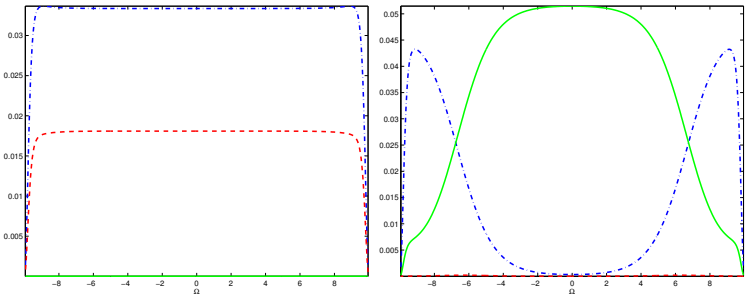

Figure 3: (Case 1) Densities of the starting state $q = 0$ (left) and the target state $q = 1$ (right) of curve 1-1 in Fig. 1. The $m_F = 1, 0, -1$ components are depicted by blue dash-dotted, green solid and red dashed lines, respectively.

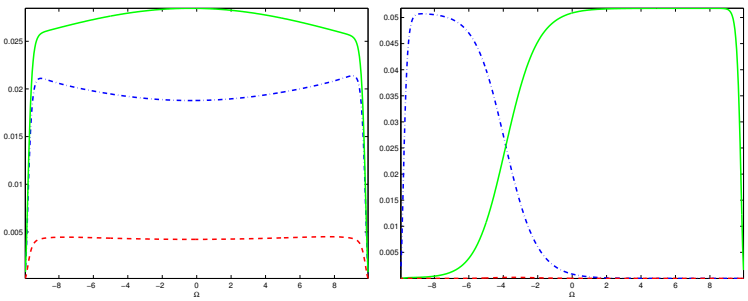

Figure 4: (Case 1) Densities of the starting state $q = 0$ (left) and the target state $q = 1$ (right) of curve 1-1-1 in Fig. 1. The $m_F = 1, 0, -1$ components are depicted by blue dash-dotted, green solid and red dashed lines, respectively.

Table 2: (Case 1) Ground state patterns of antiferromagnetic BEC (^{23}Na) with $M = 0.3$ in the constant potential.

	$q=-1$	$q=0$	$q=0.02582$	$q=0.1115$	$q=1$	$q=3$
Energy ($\tilde{\mathcal{E}}$)	5.2568	6.2568	6.2818	6.3309	6.6105	7.2114
N_{-1}	0.35	0.35	0.2673	0.07373	0.0007	0.00008
State	2C	2C	3C	2C+NS	2C+NS	MS+NS
Profile	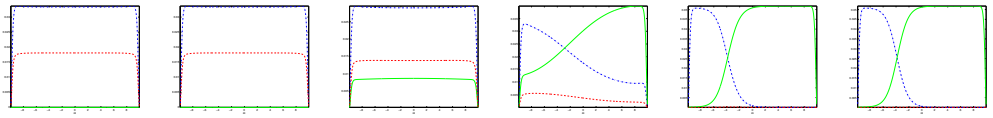					

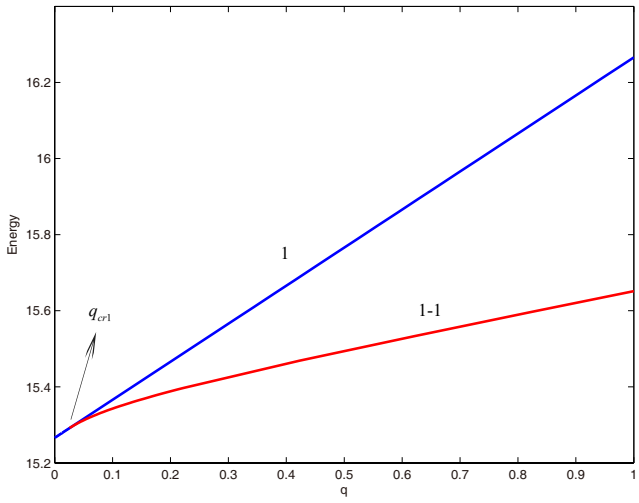

Figure 5: (Case 2) Energy curves of ^{23}Na with $M = 0.3$ in the harmonic potential. There is one bifurcation point $q_{cr1} = 0.02606$.

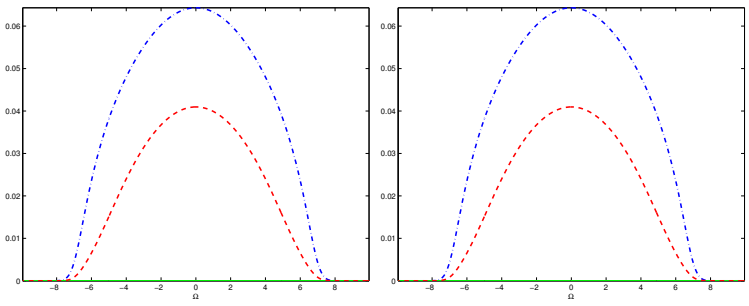

Figure 6: (Case 2) Densities of the starting state $q = 0$ (left) and the target state $q = 1$ (right) of curve 1 in Fig. 5. The $m_F = 1, 0, -1$ components are depicted by blue dash-dotted, green solid and red dashed lines, respectively.

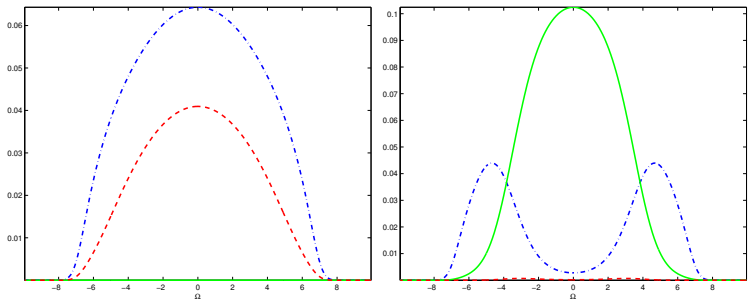

Figure 7: (Case 2) Densities of the starting state $q = 0$ (left) and the target state $q = 1$ (right) of curve 1-1 in Fig. 5. The $m_F = 1, 0, -1$ components are depicted by blue dash-dotted, green solid and red dashed lines, respectively.

Table 3: (Case 2) Ground state patterns of antiferromagnetic BEC (^{23}Na) with $M = 0.3$ in the harmonic potential.

	$q = -1$	$q = 0$	$q = 0.1537$	$q = 1$	$q = 8$
Energy ($\tilde{\mathcal{E}}$)	14.2659	15.2659	15.3686	15.6515	17.7593
N_{-1}	0.35	0.35	0.0724	0.004	0.00008
State	2C	2C	2C+NS	2C+NS	MS+NS
Profile	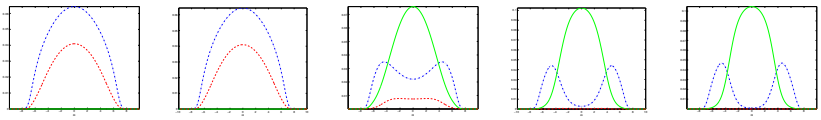				

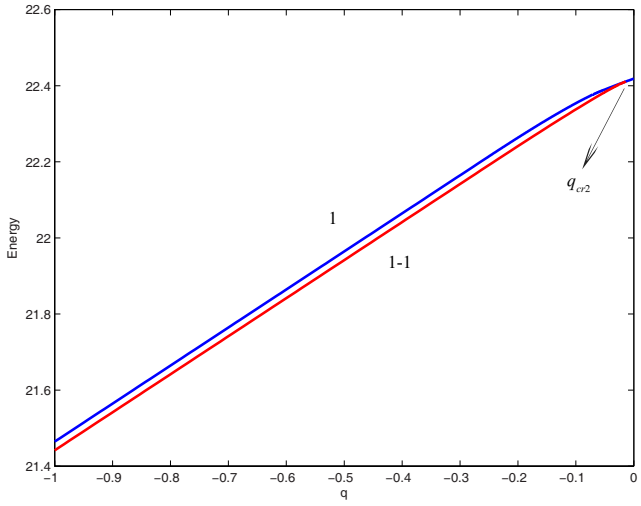

Figure 8: (Case 3) Energy curves of ^{87}Rb with $M = 0.3$ in the constant potential. There is one bifurcation point $q_{cr2} = -0.003452$.

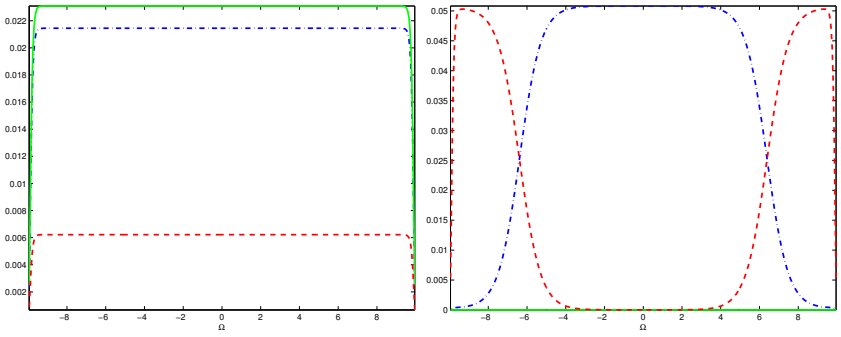

Figure 9: (Case 3) Densities of the starting state $q = 0$ (left) and the target state $q = 1$ (right) of curve 1 in Fig. 8. The $m_F = 1, 0, -1$ components are depicted by blue dash-dotted, green solid and red dashed lines, respectively.

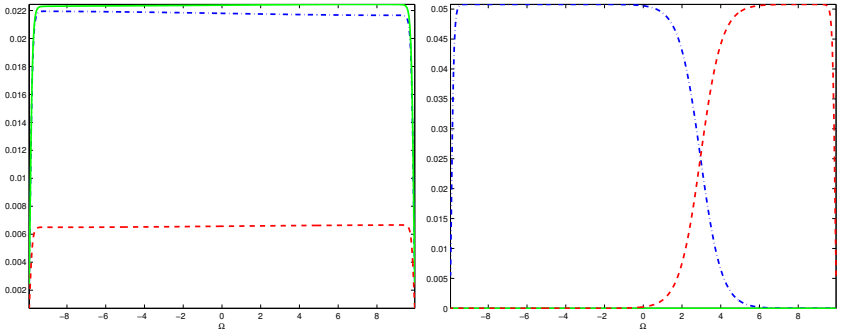

Figure 10: (Case 3) Densities of the starting state $q = 0$ (left) and the target state $q = 1$ (right) of curve 1-1 in Fig. 8. The $m_F = 1, 0, -1$ components are depicted by blue dash-dotted, green solid and red dashed lines, respectively.

Table 4: (Case 3) Ground state patterns of ferromagnetic BEC (^{87}Rb) with $M = 0.3$ in the constant potential.

	$q = -1$	$q = -0.2035$	$q = -0.01416$	$q = 0$	$q = 1$	$q = 5$
Energy ($\tilde{\mathcal{E}}$)	21.4417	22.2379	22.4109	22.4187	22.7659	23.9687
N_{-1}	0.35	0.3438	0.1337	0.1225	0.0018	0.00007
State	MS+MS	MS+MS+NS	2C+NS	3C	3C	2C$_{\{1,0\}}$
Profile	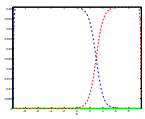	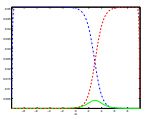	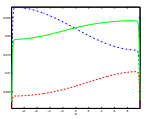	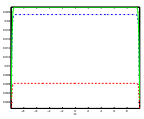	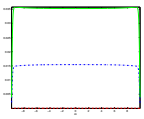	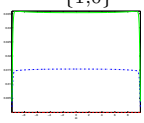

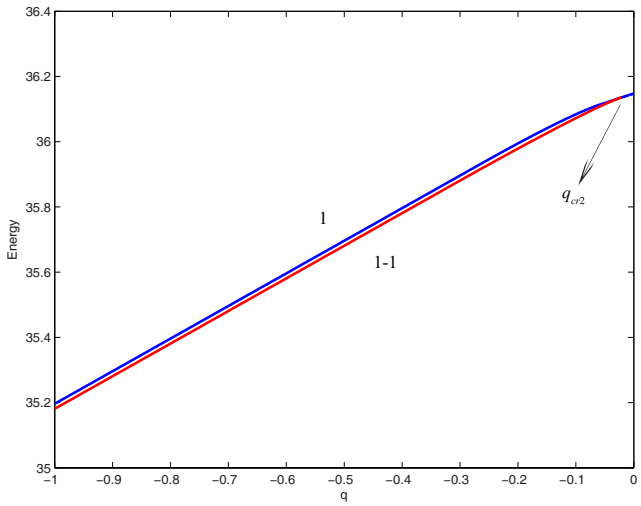

Figure 11: (Case 4) Energy curves of ^{87}Rb with $M = 0.3$ in the harmonic potential. There is one bifurcation point $q_{cr2} = -0.02125$.

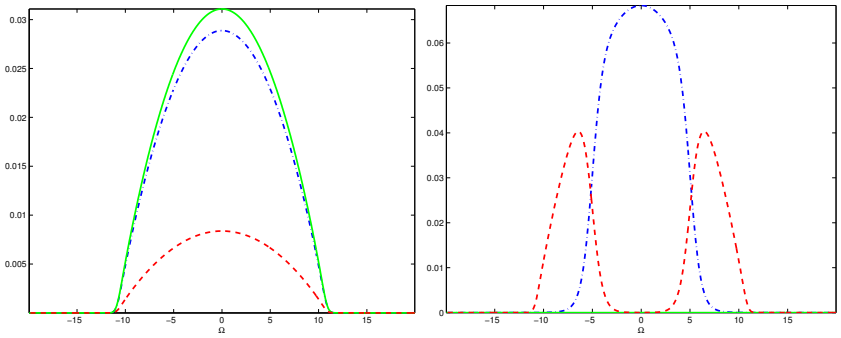

Figure 12: (Case 4) Densities of the starting state $q = 0$ (left) and the target state $q = 1$ (right) of curve 1 in Fig. 11. The $m_F = 1, 0, -1$ components are depicted by blue dash-dotted, green solid and red dashed lines, respectively.

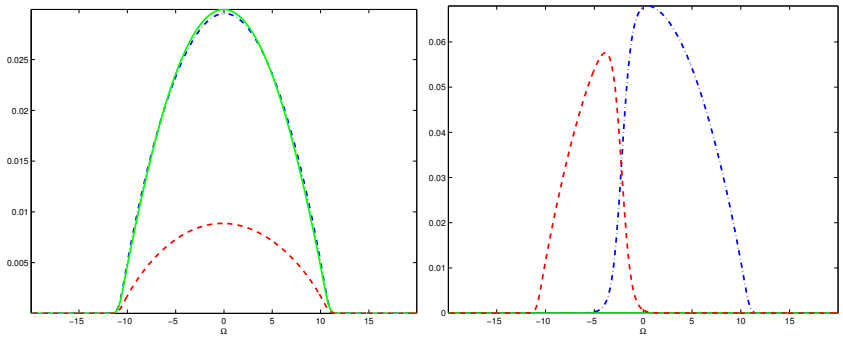

Figure 13: (Case 4) Densities of the starting state $q = 0$ (left) and the target state $q = 1$ (right) of curve 1-1 in Fig. 11. The $m_F = 1, 0, -1$ components are depicted by blue dash-dotted, green solid and red dashed lines, respectively.

Table 5: (Case 4) Ground state patterns of ferromagnetic BEC (^{87}Rb) with $M = 0.3$ in the harmonic potential.

	$q = -1$	$q = -0.06099$	$q = -0.02195$	$q = 0$	$q = 1$	$q = 5$
Energy ($\tilde{\mathcal{E}}$)	35.1809	36.1352	36.10605	36.1474	36.4957	37.6991
N_{-1}	0.35	0.2658	0.1399	0.1225	0.0021	0.00008
State	MS+MS	MS+MS+NS	2C+NS	3C	3C	$2C_{\{1,0\}}$
Profile	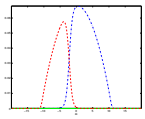	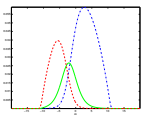	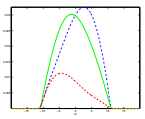	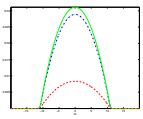	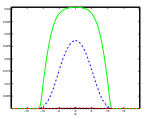	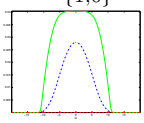

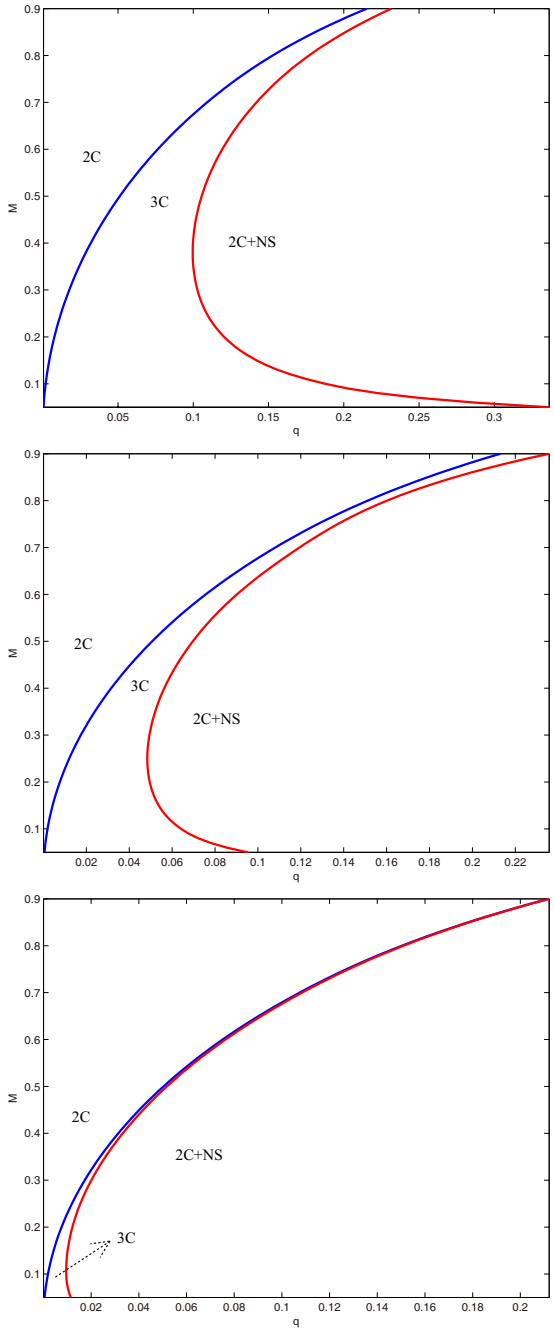

Figure 14: (semi-classical regime) The ground state phase diagram of the spin-1 ^{23}Na BEC with $\epsilon_k = 1$, $\epsilon_k = 0.5$, and $\epsilon_k = 0.1$ (from top to bottom).